

# Analysis and Comparison of Power Electronic Converters for Conventional and Toroidal Switched Reluctance Machines

Zipan Nie\*, Nigel Schofield\*

Department of Electrical and Computer Engineering, McMaster University, Hamilton, Canada

Email: \*niez4@mcmaster.ca, \*nigels@mcmaster.ca

**How to cite this paper:** Nie, Z.P. and Schofield, N. (2017) Analysis and Comparison of Power Electronic Converters for Conventional and Toroidal Switched Reluctance Machines. *Energy and Power Engineering*, 9, 241-259.

<https://doi.org/10.4236/epe.2017.94017>

**Received:** February 6, 2017

**Accepted:** April 23, 2017

**Published:** April 26, 2017

Copyright © 2017 by authors and Scientific Research Publishing Inc.

This work is licensed under the Creative Commons Attribution International License (CC BY 4.0).

<http://creativecommons.org/licenses/by/4.0/>



Open Access

---

## Abstract

Different power electronic converter topologies are introduced in this paper for both Conventional Switched Reluctance Machine (CSRSM) and Toroidal Switched Reluctance Machine (TSRM) drive systems. Their commutation, switch and diode currents, power losses, and efficiencies under over modulation operation are analyzed and compared for converter characteristics study, performance evaluation and topology selection for CSRSM and TSRM drive systems. The switch and diode silicon volumes required for each CSRSM and TSRM drives are also compared according to their corresponding currents at the equivalent machine torque versus speed operating points.

## Keywords

Power Electronic Converter, Conventional Switched Reluctance Machine, Toroidal Switched Reluctance Machine

---

## 1. Introduction

Electrical machine drive systems are widely used in different applications, e.g. traction systems, industrial drives, and home appliances. So far the maturely developed and widely applied machine drive systems comprise of brushed DC, AC induction, and AC permanent magnet machine drive systems, whose torque generation are mainly via magnetic excitation and supplemented by some reluctance torque in the case of Interior Permanent Magnet Machines (IPM). For reluctance torque based machines, the development, optimization, and public acceptances of Switched Reluctance Machines (SRM) and Synchronous Reluctance Machines (SynRM) fall behind their counterparts. However, these technologies have received much interest in recent years due to the uncertainty in permanent magnet price [1] with researchers quoting application specific advantages in-

cluding the potential for low total drive system cost, machine structure robustness and simplicity, control reliability and simplicity, high efficiency, high operation speed, and the elimination of permanent magnet materials [2]-[6] etc. For the current SRM drive systems there are some drawbacks in terms of torque density, torque ripple, and acoustic noise [2].

Due to the different torque generation mechanisms, the requirements of machine inverters for SRMs are different to other machine technologies. For this discussion SRM with a conventional winding configuration, as shown in **Figure 1(a)**, is referred to the conventional switched reluctance machine (CSRM). Although different inverter topologies for CSRM have been proposed [7], the widely used inverter topology is the asymmetric inverter as shown in **Figure 1(b)** in which unidirectional phase current is switched through the phase winding.

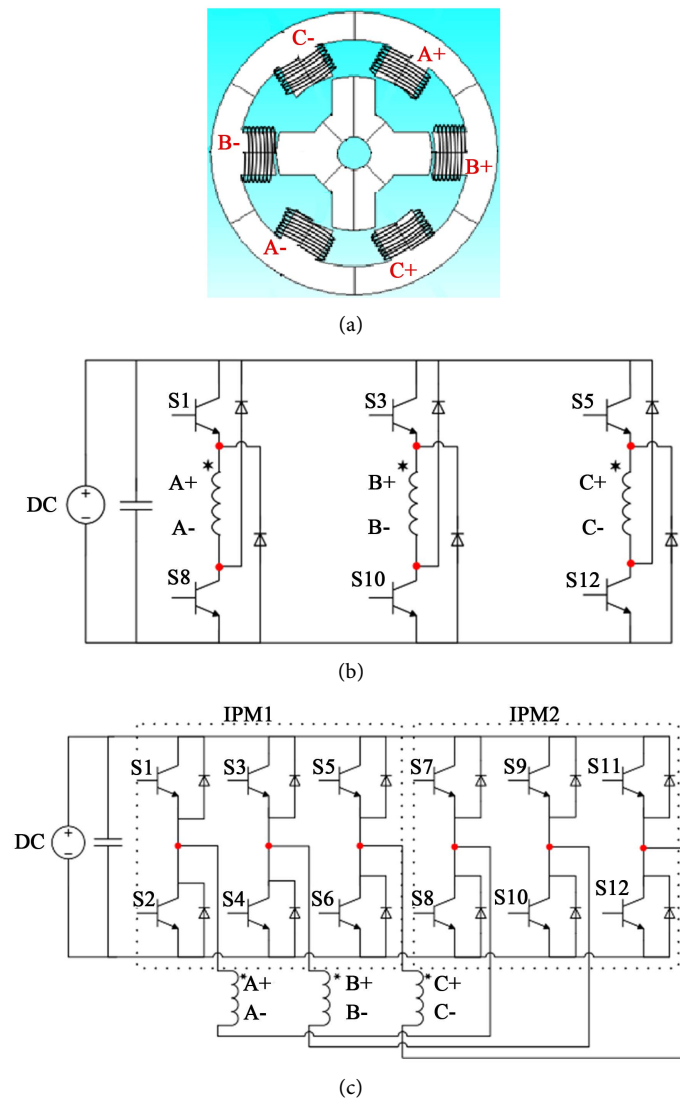


**Figure 1.** CSRM and the power electronic converters: (a) CSRM winding configuration; (b) 6 switch mode CSRM power electronic converter; (c) 12 switch mode CSRM power electronic converter.

The Toroidal Switched Reluctance Machine (TSRM) has a different winding configuration to the CSRSM [8] [9] [10], having the stator coils toroidally wound on the stator back iron, as shown in **Figure 2(a)**. Compared with CSRSMs this potentially yields better cooling and improved winding packing factor [11]. The different winding configuration of the TSRM leads to its different current paths than the CSRSM, requiring different commutations and power electronic converter topology [9] [10] [12]. Different power converter topologies and control strategies have been proposed for CSRSM and TSRM [13] [14] [15] [16] as shown in **Figure 1** and **Figure 2**. However, the silicon device specifications required by different CSRSM or TSRM drive systems have not been analyzed and compared before.

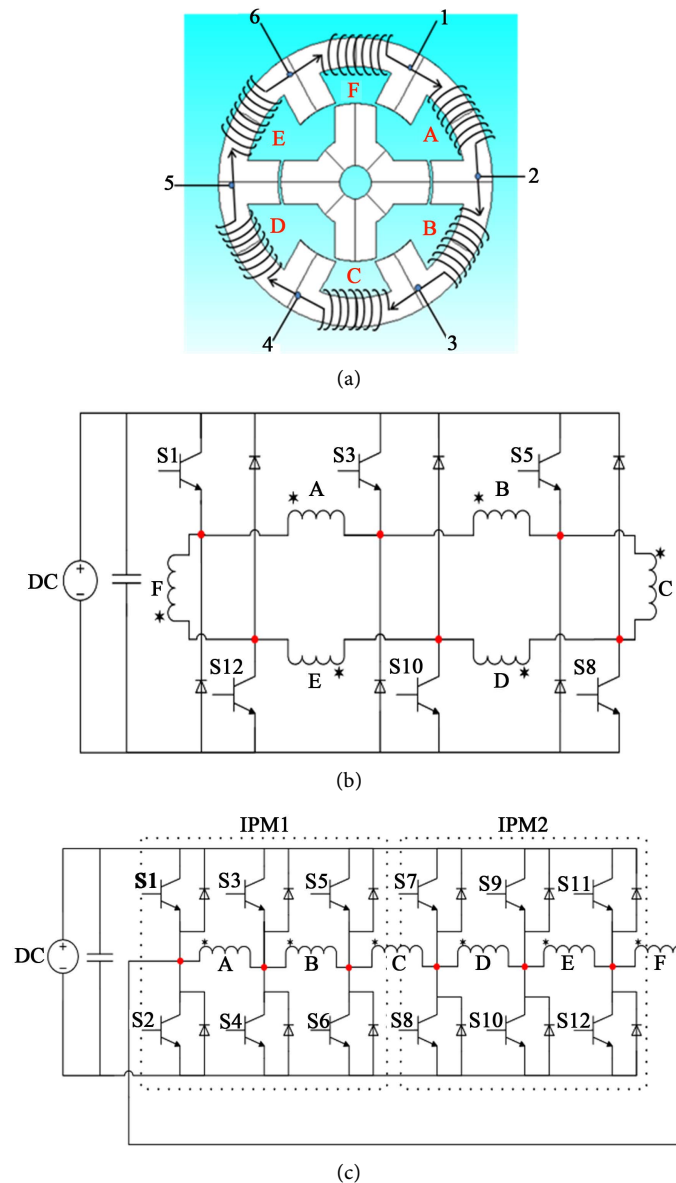


**Figure 2.** TSRM and the power electronic converters: (a) TSRM winding configuration; (b) 6 switch mode TSRM power electronic converter; (c) 12 switch mode TSRM power electronic converter.

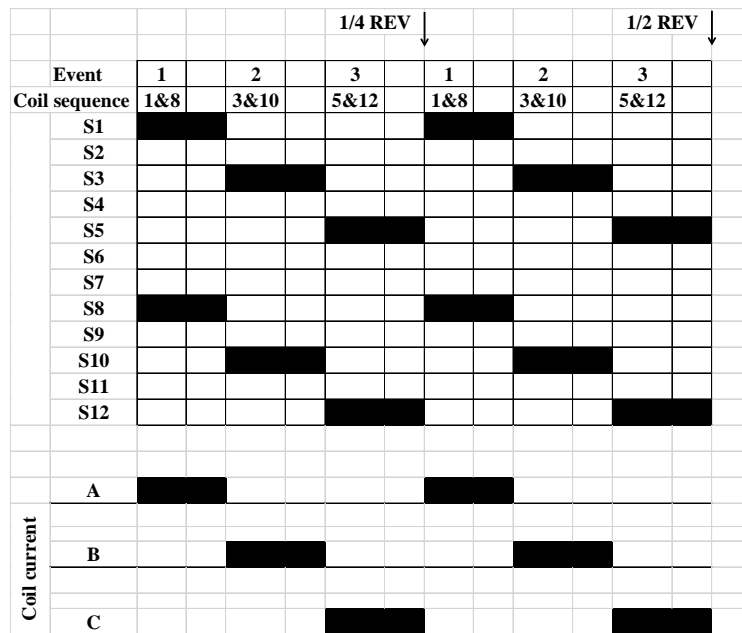
This paper presents different power electronic converters for both CSRSM and TSRM, their topologies, commutation strategies, switch and diode currents, and power dissipation of silicon devices, which can help to make references when determining the ratings of power electronic switches, diodes and evaluating the converter performance and characteristics. Experimental tests have been conducted under different DC-link voltages and different torque versus speed operating points. Analysis and comparisons have been made for device currents, power losses and efficiencies for the different power converters. The required power electronic silicon material volume is also compared among different converters. The purpose of this research is to suggest the application guideline for the inverter systems for CSRSM and TSRM, both 6SW and 12SW mode. What the similarities and differences are, containing the inverter system power losses, efficiencies, power semiconductor ratings, commutation characteristics, etc., and what the attentions should be paid under different application criteria, for example, electric vehicles, home appliances, aerospace applications, etc.

## 2. Power Electronic Converters for CSRSM and TSRM

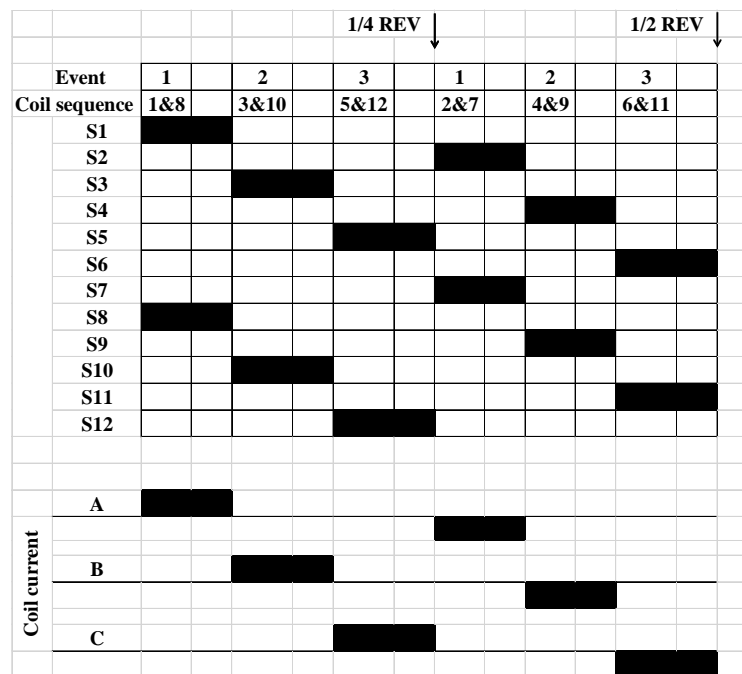
Two different power electronic converters are proposed for either the CSRSM shown in **Figure 1(a)** or TSRM shown in **Figure 2(a)**. The CSRSM power converter topologies are illustrated in **Figure 1**, in which **Figure 1(b)** shows a typical asymmetric converter, *i.e.* 6 switch mode (6SW), and **Figure 1(c)** shows a converter composed of 2x 3-phase full bridge voltage source inverters that implements a 12 switch mode (12SW). For the latter case, the 12 switch mode inverter is practically implemented via 2x IGBT Intelligent Power Modules (IPMs), IPM1 and IPM2. **Figure 2** shows two different power converter topologies driving the TSRM, **Figure 2(b)** 6 switch mode (6SW), and **Figure 2(c)** 12 switch mode (12SW), again implemented via 2x IPMs.

The switching sequences for CSRSM 6SW and CSRSM 12SW are given in **Figure 3** and **Figure 4** shows TSRM 6SW and TSRM 12SW switching sequences. Taking the CSRSM 6SW switching sequence for example, in this 4-pole SR machine there are 4 electrical periods in one mechanical revolution *i.e.* 1 electrical revolution corresponds 1/4 mechanical revolution, 1/4 REV in **Figure 3(a)**. “Event” means the instantaneous commutation state and the “Coil sequence” indicates the on-state switches shown in **Figure 1** and **Figure 2** under one commutation state. “Coil current” shows the polarity of the though coil current in the respective commutations. While for CSRSM 12SW 1 electrical revolution corresponds 1/2 mechanical revolution and the coil current is bipolar, **Figure 3(b)**. Having the same mechanical and electrical revolution relation (under 6SW and 12SW) with CSRSM, both the TSRM 6SW and TSRM 12SW have bipolar current in their coils, **Figure 4**, while the TSRM 6SW has unbalanced current in coils, different to the other systems.

The coil A current waveforms for two different CSRSM converters (6SW and 12SW) are shown in **Figure 5(a)** and **Figure 5(b)**, where the 6SW converter has unipolar current, but in the 12SW converter the coil current polarity changes in



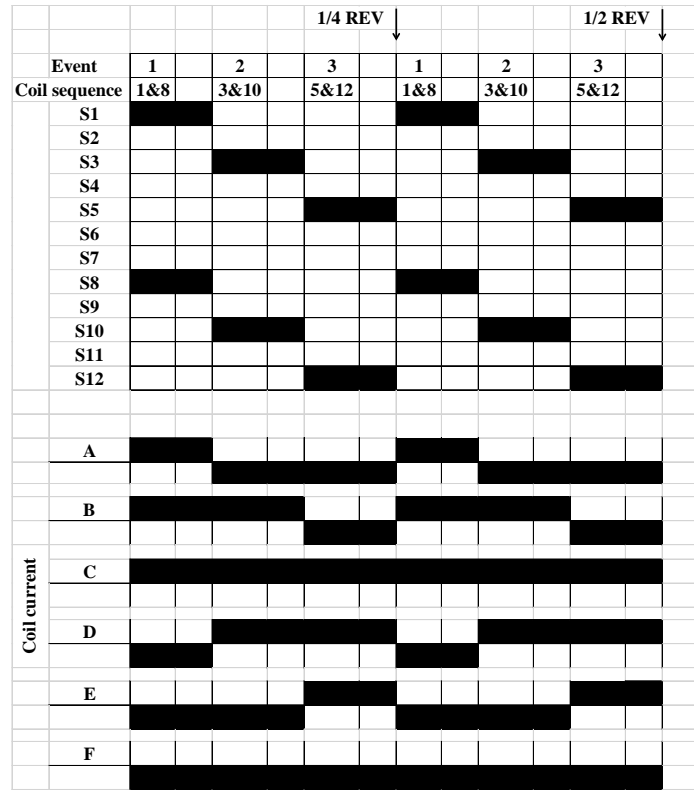
(a)



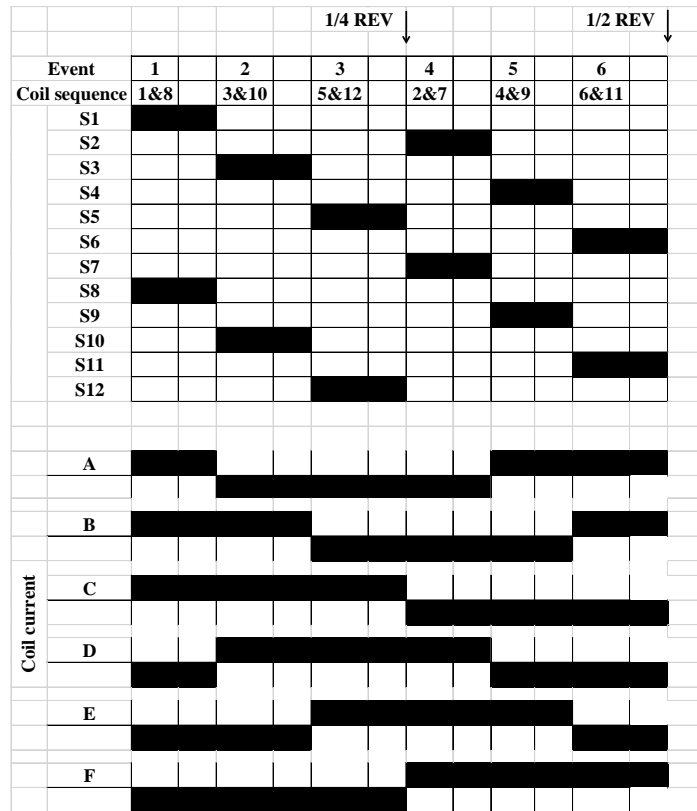
(b)

**Figure 3.** CSRMs switching sequences and corresponding coil current polarity: (a) 6 switch mode CSRMs; (b) 12 switch mode CSRMs.

every period. During the coil current increasing segment of each pulse, the currents are driven by the DC-link through switches, and during the coil current decreasing segment, the coils are discharged releasing the storage magnetic energy via the diodes. Theoretically, both the converters have the same coil current in spite of their polarity, which means the same overall power dissipation under the same operating conditions. However, in the 12SW converter the three



(a)



(b)

**Figure 4.** TSRM switching sequences and corresponding coil current polarity: (a) 6 switch mode TSRM; (b) 12 switch mode TSRM.

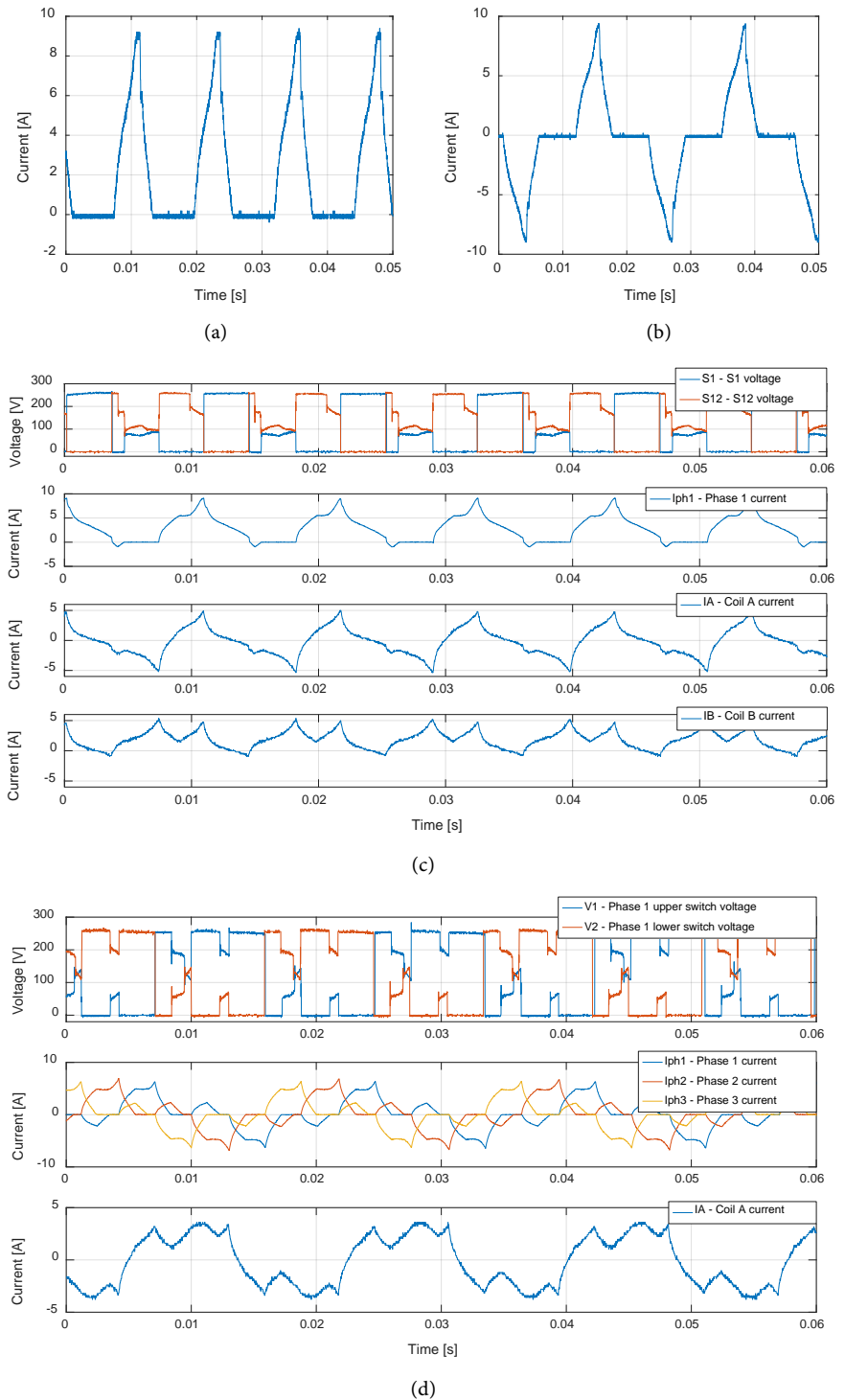


**Figure 5.** Experimental current and voltage waveforms for CSRm, TSRm, 6SW and 12SW: (a) CSRm 6SW coil A current; (b) CSRm 12SW coil A current; (c) TSRm 6SW operation waveforms; (d) TSRm 12SW operation waveforms.

coil currents go through 12 switches and diodes, while in 6SW converter currents go through 6 switches and diodes—same overall power dissipation on different numbers of switches and diodes indicating more even and uniform power dissipation on the power silicon cooling surface of 12SW than 6SW converter.

Another characteristics of the CSRSM power converters is that their coils are independently connected to the DC bus, which means from the converter side, there is no mutual effects between different phases and the current waveform of each coil can be studied and analyzed separately. That is also called the decoupled characteristics in CSRSM while in TSRM the mutual effects among different phases counts. From the machine torque generation view, in terms of CSRSM it is the coil self-inductance variation that contributes torque while in TSRM both the self- and mutual- inductances work.

There are two different converter topologies for the TSRM drive system proposed in this paper. **Figure 2(b)** shows the topology for 6SW TSRM converter, and its current waveforms for different coils and phases are by nature not all the same, as shown in **Figure 5(c)**, resulting in the switches and diodes currents unbalance in the converter that means the ratings and losses among different switches and diodes are not all the same. Also the mutual effects or coupling among neighboring coils, and the diode voltage clamping effects introduce transient voltage states during the switch commutations, which does not exist in CSRSM converters. But the switches transient voltages are lower than the DC-link voltage implying the same voltage rating of switches and diodes compared with CSRSM converters.

In the 12SW TSRM power electronic converter, **Figure 2(c)**, both the coil currents and phase currents are balanced, which means different coil and phase currents have the same waveform shapes but with certain phase shift among them, as shown in **Figure 5(d)**. Similar with 6SW converter, coupling among phases and hence the switch transient voltage states also exist.

### 3. Semiconductor Device Ratings

The semiconductor device ratings are constrained and determined by their electrical, material, mechanical, and thermal properties, design, and manufacture processes etc., among which the thermal properties are comparatively dominant on the rating restrictions. Thermal properties of a device are determined by its power loss and heat transfer characteristics. Power losses in a semiconductor device include conduction losses, switching losses, diode recovery losses, gate drive losses and blocking losses, which introduce heat generation on device chips. Among these losses blocking losses are normally neglected [17]. Heat transfer characteristics are dependent on the material applied and the switch geometry design.

According to the machine drive system application, Insulated Gate Bipolar Transistors (IGBT) and Metal Oxide Semiconductor Field Effect Transistors (MOSFETs) are widely used currently and hence analyzed in this paper. General losses mechanism and calculation methods are introduced here. While the switches ratings are highly dependent on the machine drive type, switching schemes etc.

During the switch-on state, currents go through switches junctions and dissipate joule heat so that the temperature growth occurs at the junction (account-

ing for the majority), the internal leads and contacts, and the external connectors. The current through the switch is constrained below some certain value to prevent the thermal breakdown and latch up [18]. Take the IGBT for example; two current restrictions are the maximum continuous collector current and a maximum peak current pulse whose magnitude, width and some other conditions are pre-defined by manufactures [19].

During the off-state, at least one junction is reverse-biased to hold the voltage which has an upper limitation equal to the breakdown voltage of the device junction [18]. That is called maximum rated collector-emitter voltages which is dependent on junction temperatures [19].

The silicon volume used in switch/diode is mainly dependent on the power dissipation and hence the RMS or average currents, maximum rated collector-emitter voltages (the thickness of switch dies), material thermal conductivity, and the switch and diode dies layouts.

### 3.1. Conduction Losses

During the conduction mode, the IGBT switch can be modelled via an equivalent circuit in which a DC voltage source and an on-state resistance are connected in series [19], [20]:

$$u_{CE}(i_C) = u_{CE0} + r_C \cdot i_C \quad (1)$$

where  $u_{CE}$  is the collector-emitter voltage,  $u_{CE0}$  is the modelled DC voltage source,  $r_C$  is the equivalent on-state resistance, and  $i_C$  is the collector current.

The IGBT instantaneous conduction loss is [20]:

$$p_{CI}(t) = u_{CE}(t) \cdot i_C(t) = u_{CE0} \cdot i_C(t) + r_C \cdot i_C^2(t) \quad (2)$$

and hence the IGBT average conduction loss in one switching period is [20]:

$$P_{CA} = \frac{1}{T_{sw}} \int_0^{T_{sw}} p_{CI}(t) dt = u_{CE0} \cdot I_{cav} + r_C \cdot I_{crms}^2 \quad (3)$$

where  $T_{sw}$  is the switching period,  $I_{cav}$  is the average current during this period and  $I_{crms}$  is the RMS current during the integral period.

The diode conduction losses  $P_{CAD}$  can be calculated in the same way. Similarly, the MOSFET conduction loss can be modelled similarly with that of the IGBT, however, for a MOSFET  $u_{CE0}$  is zero [20].

### 3.2. Switching Losses and Reverse Recovery Losses

Switching losses are characterized for IGBTs under worst case operation [19] [20], and similar with MOSFET devices [21]. The turn-on loss is the sum of switch-on energy without the effects from the free-wheeling diode ( $E_{onTi}$ ) and the energy caused by diode reverse recovery ( $E_{onTrr}$ ) [19] [20]. Turn-on switching energy can be calculated from [19] [20] [21]:

$$E_{on} = \int_0^{tri+tfu} (u_{CE}(t) \cdot i_C(t)) dt = E_{onTi} + E_{onTrr} = U_{DD} \cdot I_{Con} \cdot \frac{tri+tfu}{2} + Q_{rr} \cdot U_{DD} \quad (4)$$

where  $U_{DD}$  is the converter supply voltage,  $I_{Con}$  is the on-state collector current,  $tri$  is the current rise time,  $tfu$  is the voltage fall time, and  $Q_{rr}$  is the reverse recovery charge.

Turn-off switching energy is given by [19] [20] [21]:

$$E_{off} = \int_0^{tru+tfi} (u_{CE}(t) \cdot i_C(t)) dt = U_{DD} \cdot I_{Coff} \cdot \frac{tru + tfi}{2} \quad (5)$$

where  $I_{Coff}$  is the off-state collector current,  $tru$  is the voltage rise time, and  $tfi$  is the current fall-time.

Reverse recovery energy is given by [19] [20] [21]:

$$E_{rec} = \int_0^{tri+tfu} u_D(t) \cdot i_F(t) dt = \frac{1}{4} \cdot Q_{rr} \cdot U_{Drr} \quad (6)$$

where  $u_D$  is the voltage across the diode,  $i_F$  is the current through the diode, and  $U_{Drr}$  is the voltage across the diode during the reverse recovery.

### 3.3. Gate Drive Losses

In MOSFETs and IGBTs the semiconductor layers among gate, drain (collector), and source (emitter) terminals introduce gate to drain (collector) capacitance, gate to source (emitter) capacitance and drain (collector) to source (emitter) capacitance, which determine not only the switching transient but also the gate charge, and hence the gate losses during the turn-on and turn-off transients [22]. Although compared with conduction and switching losses gate drive losses are small, investigation on it is necessary to an integral switching transient study.

The required gate charge increases with the switch current rating and voltage rating, between which current rating is the more decisive factor. Gate driver losses can be calculated by [22]:

$$P_{gate} = V_{CC} \cdot Q_g \cdot f_{sw} \quad (7)$$

where  $V_{CC}$ -Driver supply voltage,  $Q_g$ -Total gate charge to drive the switch, and  $f_{sw}$ -switching frequency. The driver supply voltage and total gate charge are normally given by the manufacturer.

### 3.4. Total Losses

The total power losses in a semiconductor device contain conduction losses, switching losses, reverse recovery losses and gate drive losses (neglecting the blocking losses):

$$P_{total} = P_{CA} + P_{CAD} + (E_{on} + E_{off} + E_{rec} + V_{CC} \cdot Q_g) \cdot f_{sw} \quad (8)$$

Among them conduction losses, switching losses, and reverse recovery losses are generated on the switch and diode chip which are fitted in some certain kind of package and adhered on heat sinks forming the heat transfer path for heat releasing. While the gate drive losses mainly occur inside the gate drive chips and does not share the same heat transfer path. When the converter efficiency is analyzed, the gate drive losses are necessarily considered. While gate drive losses do not contribute the junction temperature changes hence it will not be counted

when converter power circuitry thermal performances and current constraints are evaluated.

## 4. Experiment and Results Analysis

The CSRSM and TSRM power electronic converters are implemented with the experimental facility containing an Arduino DUE R3 as the controller, 2 PM50RLA060 integrated power modules (3-phase full-bridges IGBT module) from Powerex and their corresponding driver boards, Powerex BP7B, load dynamometer machine, CSRSM and TSRM prototypes, power supplies, torque transducer and accessory circuit boards for logic signal conversion and isolation. In terms of measurements, a Tektronix oscilloscope MDO3024, Metrix differential probe MX 9003, and LEM LA 55-P current transducers are used to capture voltage, current and torque waveforms. The experimental facility is given in **Figure 6**.

### 4.1. Comparison between CSRSM 12SW and CSRSM 6SW

Switch and diode current, power losses and converter efficiencies are compared between CSRSM 12SW and CSRSM 6SW for different load operation points. For the over modulation operation, switching losses and reverse recovery losses can be neglected and only conduction losses are taken into consideration. The power dissipations of switches and diodes are dependent on their corresponding RMS currents and average currents, as defined in Equation (3). A water cooling cold plate is used in the experiment set-up to keep the IGBT module case temperature at 20°C. Thus it is assumed that the parameters applied in Equation (3) are under the condition of 25°C junction temperature.

**Figure 7(a)** and **Figure 7(b)** show the torque versus speed characteristics, and the switch and diode RMS currents versus speed for different operating points of the CSRSM 6SW and CSRSM 12SW drive systems at DC-link voltages of 150 and 300 V.

To normalize the experimental results in **Figure 7(a)** and **Figure 7(b)**, the torque to switch and torque to diode RMS current ratios are calculated and compared quantitatively. **Figure 7(c)** and **Figure 7(d)** show these ratios versus the machine rotational speed at DC-link voltages of 150 and 300 V.

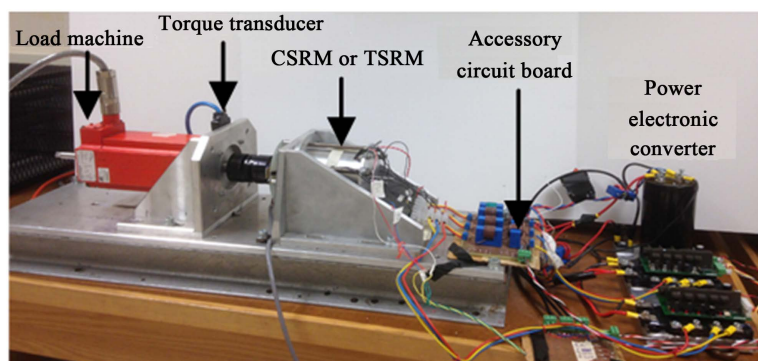
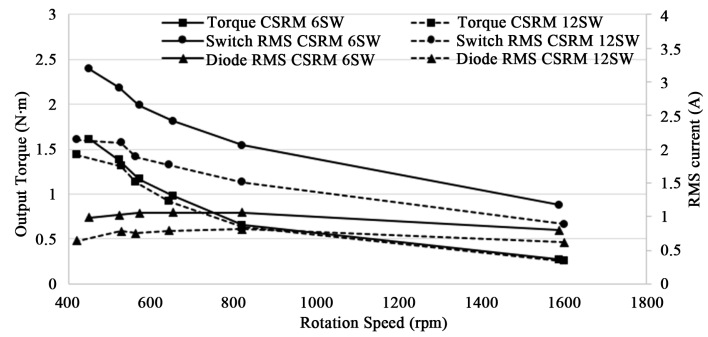
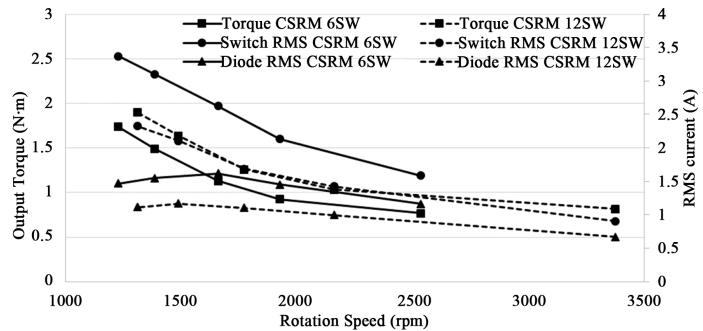


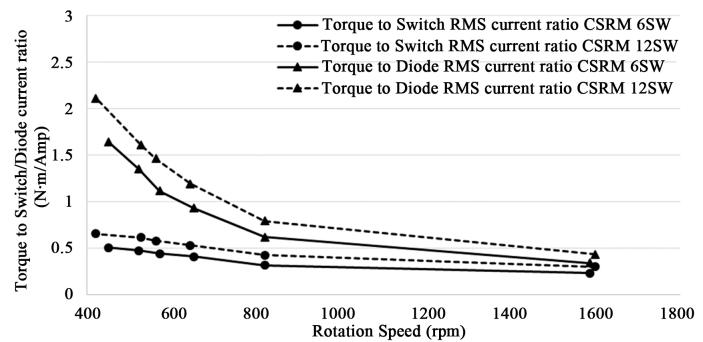
**Figure 6.** Experimental test facility.



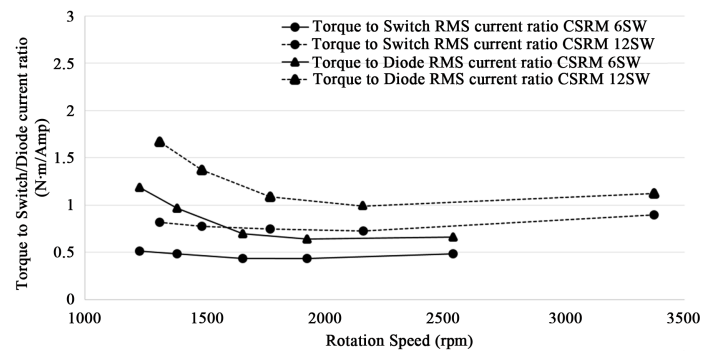
(a)



(b)



(c)



(d)

**Figure 7.** Experimental test results for the CSRM: (a) Torque, diode and switch RMS current versus rotational speed at a DC bus voltage = 150 V; (b) Torque, diode and switch RMS current versus rotational speed at a DC bus voltage = 300 V; (c) Torque to switch and torque to diode RMS current ratio versus rotational speed at a DC bus voltage = 150 V; (d) Torque to switch and torque to diode RMS current ratio versus rotational speed at a DC bus voltage = 300 V.

**Figure 7(c)** and **Figure 7(d)** denote higher torque to switch and torque to diode RMS current ratios for the CSRSM 12SW converter than the CSRSM 6SW converter, which means that to generate the same torque the RMS currents per switch and diode are lower in CSRSM 12SW than those in CSRSM 6SW. However, these ratios of CSRSM 12SW are not simply the twice of those for CSRSM 6SW, even the switch and diode numbers in CSRSM 12SW doubling those in CSRSM 6SW, but vary under different operation points and DC-link voltages. Also in either CSRSM 12SW or CSRSM 6SW under the same operation point the torque versus diode RMS current ratios are more than the torque versus switch RMS current ratios, which is understandable because the excitation currents via switches are more than the freewheeling currents through diodes as shown in **Figure 5(a)** and **Figure 5(b)**. In semiconductor devices the switches are normally designed to have the same current and voltage ratings with their respective freewheeling diodes so only the torque versus switch RMS current ratios are investigated and compared for simplification. On the contrary if the equivalent current rating requirement in switch and its freewheeling diode are not considered, for this specific and some other certain applications the freewheeling diodes can be designed with lower current ratings than the corresponding switches to save the silicon materials and hence the costs.

Under the DC-link voltage of 150V the difference between the torque versus switch RMS current ratios of both CSRSM 12SW and CSRSM 6SW is not sound, 0.65 N·m/Amp and 0.5 N·m/Amp at the highest torque points on **Figure 7(c)**. While this difference is enlarged when the DC-link voltage becomes 300V that the ratios are 0.83N.m/Amp and 0.5 N·m/Amp at the highest torque points on **Figure 7(d)**. For the torque to diode RMS current ratios of both CSRSM 12SW and CSRSM 6SW under 300V DC-link voltage, the values are 1.67 N·m/Amp and 1.17N.m/Amp respectively. Assume that the switch or diode silicon volume required is proportional to the joule heat, hence the square of the RMS current through themselves. Between CSRSM 6SW and CSRSM 12SW and under the same machine operating point, the former drive system requires 2.79 times silicon volume for each switch and 2.09 times silicon volume for each diode. However, the total switches number of CSRSM 6SW is half the CSRSM 12SW so that the total switch and diode silicon volume for CSRSM 6 SW is 1.39 times and 1.04 times of those for CSRSM 12 SW.

From the current waveforms observation in **Figure 5(a)** and **Figure 5(b)**, the switch conduction segments account for 1/3 of the total period in CSRSM 6SW and 1/6 of the total period in CSRSM 12SW. The switch RMS currents measured from the test setup are the switch RMS current during the total electrical period, while under the steady state operation the junction temperature hits the peak at the every ends of the switch conduction segments, which means that although the switch RMS currents over the whole electrical period provide a reference for the converter switch RMS current ratings, the switch RMS currents during the every conduction segments should also be considered. However this situation only occurs under low speed that the switching period is compared to the silicon

junction thermal time constant. Under this situation, the switches and diodes in CSRSM 6SW and CSRSM 12SW require the same current ratings if the switch and diode RMS currents over the conduction segments are considered although the switches and diodes number in CSRSM 12SW doubles that of CSRSM 6SW. In this paper the RMS current of the whole electrical period is considered assuming that the machine rotational speed is not low enough hence the switch period is not compared to the silicon junction thermal time constant.

Defined in Equation (3), switch and diode power dissipations are dependent on both RMS current and average current through them. **Figure 8** shows the switch and diode average currents during one commutation state. Under similar machine torque versus speed operating points, CSRSM 12SW has lower switch and diode average current than CSRSM 6SW, approximate the half, which is easy to be understood because CSRSM 12SW switch current electrical period doubles that of CSRSM 6SW while their conduction segment currents are the same.

**Table 1** shows the total power dissipations and their respective efficiencies under different operation points. No significant difference occurs between CSRSM 6SW and CSRSM 12SW.

**Table 1.** CSRSM 6SW and 12SW power electronic converter power losses and efficiencies at different operating points.

	Rotational speed (rpm)	DC-bus input power (W)	Power losses (W)	Efficiency (%)
150 V 12SW	1600.0	162.3	6.5	96
	819.7	247.5	9.9	96
	643.8	354.0	10.9	96
	561.8	321.0	11.2	96
	526.3	276.9	12.3	95
	420.2	516.0	12.1	97
150 V 6SW	1587.3	195.9	5.8	97
	819.7	363.0	9.3	97
	652.2	399.0	10.4	97
	571.4	351.0	11.1	96
	521.7	459.0	12.0	97
	449.8	444.0	12.9	97
300 V 12SW	3372.7	192.3	6.9	96
	2159.1	223.8	10.6	95
	1770.4	272.4	12.0	95
	1485.5	318.0	14.0	95
	1310.3	345.0	14.7	95
	2533.8	267.0	8.4	96
300 V 6SW	1924.3	246.3	10.9	95
	1657.9	408.0	12.7	96
	1382.8	429.0	13.9	96
	1227.2	543.0	14.6	97

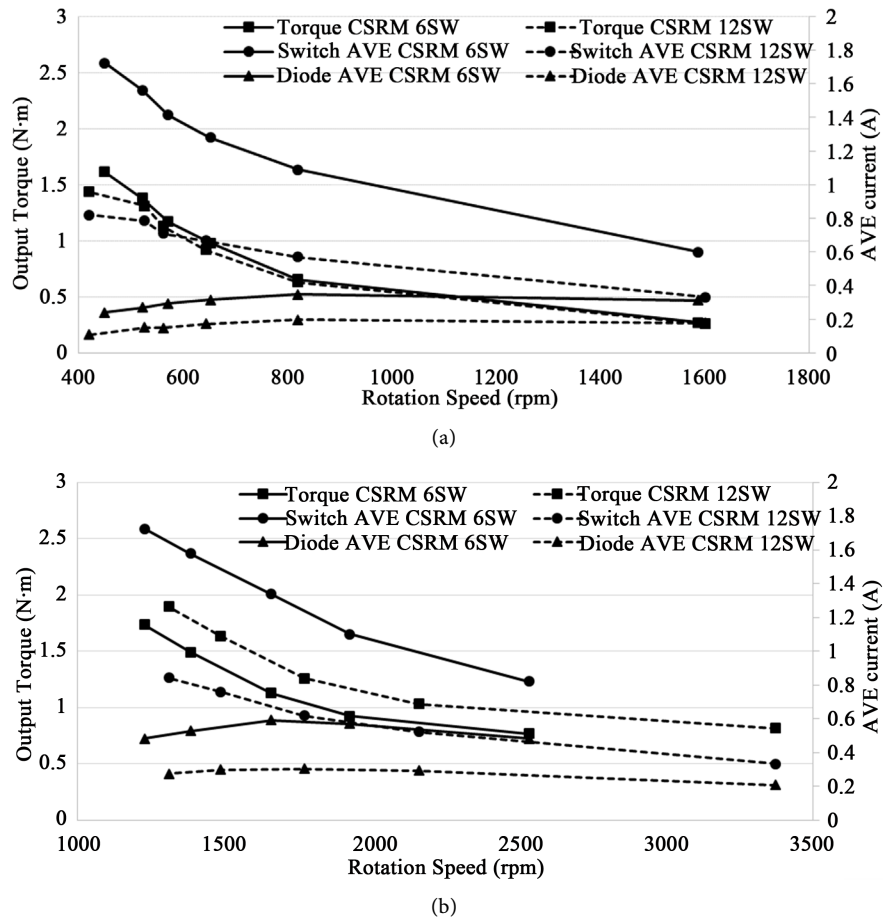


**Figure 8.** Test results for torque, diode and switch average (AVE) current versus rotational speed for the CSRMs: (a) DC bus voltage = 150 V; (b) DC bus voltage = 300 V.

#### 4.2. Comparison between TSRM 12SW and CSRM 12SW

Symmetric characteristics is an advantage of TSRM 12SW over TSRM 6SW and it results in a symmetric design of the power electronic converters (in terms of switch and diode ratings, layout and cooling system design etc.). Consequently, switch and diode current, power losses and converter efficiencies are compared between the TSRM 12SW, the candidate from TSRM family, and CSRM 12SW under different operation points. Similarly, only conduction losses are taken into consideration, and the power dissipations of switches and diodes are dependent on their corresponding RMS currents and average currents.

**Figure 9** shows the normalized switch and diode RMS current experimental results, *i.e.* the torque to switch and the torque to diode RMS current ratios for CSRM 12SW and TSRM 12SW.

When the DC-link voltage is 150 V there is no significant difference in terms of the torque to switch RMS current, while more diode RMS current is required in CSRM 12SW system. However, when the DC-link voltage is 300 V, the CSRM 12SW system requires less RMS switch and diode currents than TSRM 12SW for equivalent torque output. A higher DC-link voltage is usually selected to have a better power output capability under the same current limitation. When 300V

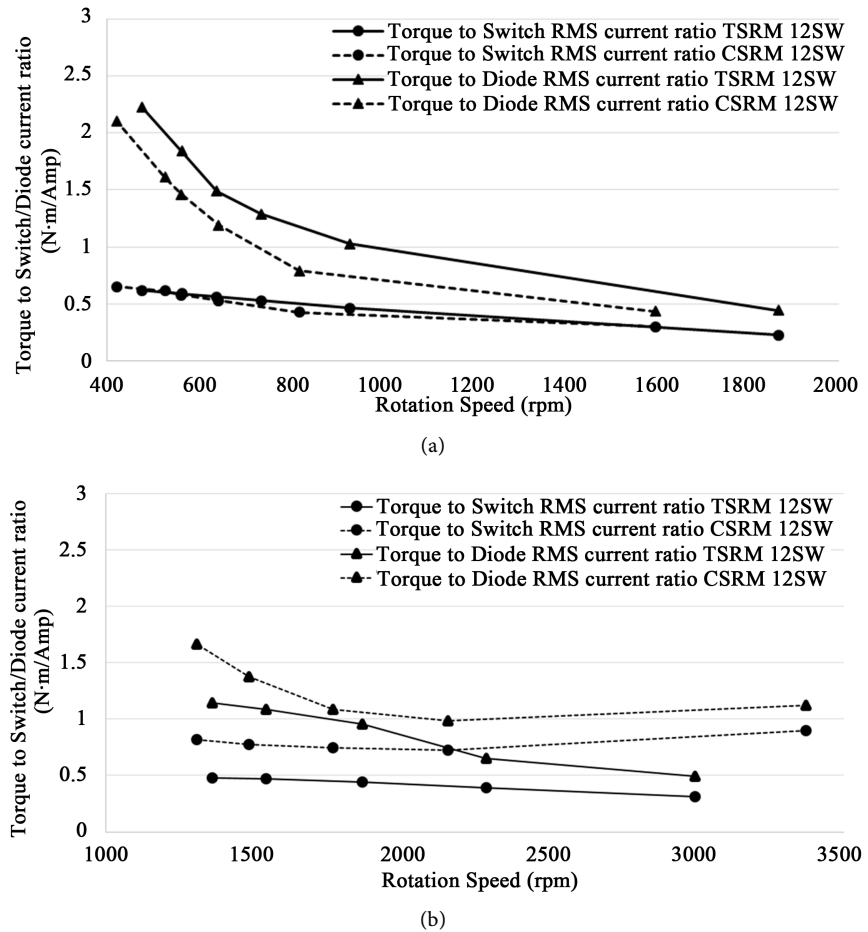


**Figure 9.** Test results for torque, diode and switch RMS current ratio versus rotational speed for both the CSR and TSRM: (a) DC bus voltage = 150V; (b) DC bus voltage = 300 V.

DC is selected, **Figure 9(b)**, the highest torque points (around 1300rpm) 1.46 times switch RMS current and 1.8 times diode RMS current are required for the TSRM 12SW than those in CSR 12SW which indicates that more silicon volume is required. Assume that the switch or diode silicon volume required is proportional to the joule heat, hence the square of the RMS current. Comparison between CSR 12 SW and TSRM 12 SW identifies that to drive the same torque output, TSRM 12SW requires respectively 2.13 times and 3.24 times switch and diode silicon volume compared with CSR 12SW.

**Table 2** shows the total power dissipations and their respective efficiencies under different operating conditions and DC-link voltages for TSRM 12SW. Comparison between TSRM 12SW in **Table 2** and CSR 12SW in **Table 1** shows that there is no significant difference in terms of power losses and efficiencies at similar operating conditions.

### 5. Conclusion

Assuming that the CSR and TSRM have equivalent performance, a comparison is made between the TSRM 12SW, CSR 12SW and CSR 6SW (as a bench

**Table 2.** TSRM 12SW power electronic converter power losses and efficiencies under different operating points.

	Rotational speed (rpm)	DC-bus input power (W)	Power losses (W)	Efficiency (%)
150V 12SW	1869.2	137.1	6.7	95
	930.2	303.0	10.9	96
	736.2	408.0	12.6	96
	639.0	483.0	13.9	97
	562.9	537.0	14.1	97
	475.4	636.0	15.6	97
	2997.0	163.5	9.1	94
300V 12SW	2288.3	224.4	12.4	94
	1869.2	363.0	14.5	96
	1544.4	507.0	16.9	96
	1362.1	540.0	19.4	96

mark) systems based on power electronic loss and operational performances. It has been demonstrated that they have similar total power dissipation and efficiency under similar torque versus speed operating points. While, due to the fact that the switch number in CSRSM 12SW is double that in CSRSM 6SW, power losses in CSRSM 12SW are more uniformly distributed than those in CSRSM 6SW (twice the cooling surface). As a consequence, this leads to a better cooling performance and potentially increases the drive capability. Moreover, the RMS and average currents through each switch and diode in CSRSM 12SW are less than those in CSRSM 6SW, which also indicates higher drive capability in CSRSM 12SW. However, the gate drive number of CSRSM 12SW doubles that of CSRSM 6SW. The silicon volume required for switches and diodes are also compared between CSRSM 6SW and CSRSM 12SW converters, and between CSRSM 12SW and TSRM 12SW converters.

## Acknowledgements

The authors acknowledge the Canada Excellence Research Chairs (CERC) program, Natural Sciences and Engineering Research Council of Canada (NSERC) Automotive Partnership Canada (APC) for support of Mr. Nie's Ph.D. Studentship.

## References

- [1] Kramer, M.J., McCallum, R.W., Anderson, I.A. and Constantinides, S. (2012) Prospects for Non-Rare Earth Permanent Magnets for Traction Motors and Generators. *The Journal of the Minerals, Metals & Materials Society (TMS)*, **64**, 752-763. <https://doi.org/10.1007/s11837-012-0351-z>
- [2] Chau, K.T. (2015) *Electric Vehicle Machines and Drives: Design, Analysis and Application*. John Wiley & Sons Ltd., Singapore. <https://doi.org/10.1002/9781118752555>

- [3] Yang, Y., Schofield, N. and Emadi, A. (2015) Double-Rotor Switched Reluctance Machine (DRSRM). *IEEE Transactions on Energy Conversion*, **30**, 671-680. <https://doi.org/10.1109/TEC.2014.2378211>
- [4] Yang, Y., Schofield, N. and Emadi, A. (2016) Double-Rotor Switched Reluctance Machine Design, Simulations, and Validations. *IET Electrical Systems in Transportation*, **6**, 117-125.
- [5] Yang, Y., Schofield, N. and Emadi, A. (2016) Integrated Electromechanical Double-Rotor Compound Hybrid Transmissions for Hybrid Electric Vehicles. *IEEE Transactions on Vehicular Technology*, **65**, 4687-4699. <https://doi.org/10.1109/TVT.2015.2487301>
- [6] Schofield, N., Long, S.A., Howe, D. and McClelland, M. (2009) Design of a Switched Reluctance Machine for Extended Speed Operation. *IEEE Transactions on Industry Applications*, **45**, 116-122.
- [7] Vukosavic, S. and Stefanovic, V.R. (1991) SRM Inverter Topologies: A Comparative Evaluation. *IEEE Transactions on Industry Applications*, **27**, 1034-1047. <https://doi.org/10.1109/28.108453>
- [8] Marlow, R., Schofield, N. and Emadi, A. (2014) A Continuous Toroidal Winding SRM with 6 or 12 Switch DC Converter. 2014 *IEEE Energy Conversion Congress and Exposition (ECCE 2014)*, Pittsburgh, 14-18 September 2014, 3826-3833. <https://doi.org/10.1109/ECCE.2014.6953921>
- [9] Lee, J.Y., Lee, B.K., Sun, T., Hong, J.P. and Lee, W.T. (2006) Dynamic Analysis of Toroidal Winding Switched Reluctance Motor Driven by 6-Switch Converter. *IEEE Transactions on Magnetics*, **42**, 1275-1278.
- [10] Lee, J.Y., Lee, B.K., Lee, J.J. and Hong, J.P. (2005) A Comparative Study of Switched Reluctance Motors with Conventional and Toroidal Windings. *IEEE International Conference on Electric Machines and Drives*, San Antonio, 15-15 May 2005, 1675-1680.
- [11] Marlow, R. (2016) Thermal Management for a Switched Reluctance Machine. Ph.D. Thesis, McMaster University, Hamilton. <https://macsphere.mcmaster.ca/bitstream/11375/18721/2/Thesis%20-%20R.%20Marlow%2012-29-15.pdf>
- [12] Marlow, R., Schofield, N. and Emadi, A. (2015) A Continuous Toroidal Winding SRM with 6- or 12-Switch DC Converter. *IEEE Transactions on Industry Applications*, **52**, 189-198. <https://doi.org/10.1109/TIA.2015.2474838>
- [13] Ye, J., Malysz, P. and Emadi, A. (2014) A Fixed-Switching-Frequency Integral Sliding Mode Current Controller for Switched Reluctance Motor Drives. *IEEE Journal of Emerging and Selected Topics in Power Electronics*, **3**, 381-394.
- [14] Neuhaus, C.R., Fuengwarodsakul, N.H. and De Doncker, R.W. (2008) Control Scheme for Switched Reluctance Drives with Minimized Dc-Link Capacitance. *IEEE Transactions on Power Electronics*, **23**, 2557-2564. <https://doi.org/10.1109/TPEL.2008.2002086>
- [15] Liu, X., Zhu, Z.Q., Hasegawa, M., Pride, A., Deohar, R., Maruyama, T. and Chen, Z. (2011) DC-link Capacitance Requirement and Noise and Vibration Reduction in 6/4 Switched Reluctance Machine with Sinusoidal Bipolar Excitation. 2011 *IEEE Energy Conversion Congress and Exposition (ECCE 2011)*, Phoenix, 17-22 September 2011, 1596-1603. <https://doi.org/10.1109/ECCE.2011.6063973>
- [16] Ye, J., Bilgin, B. and Emadi, A. (2015) An Extended-Speed Low-Ripple Torque Control of Switched Reluctance Motor Drives. *IEEE Transactions on Power Electronics*, **30**, 1457-1470.

<https://doi.org/10.1109/TPEL.2014.2316272>

- [17] Williams, B.W. (1992) Power Electronics: Devices, Drivers, Applications, and Passive Components. McGraw-Hill, New York.
- [18] Mohan, N., Undeland, T.M. and Robbins, W.P. (2002) Power Electronics: Converters, Applications, and Design. 3rd Edition, John Wiley & Sons, New York
- [19] ABB (2013) Applying IGBTs.  
[https://library.e.abb.com/public/ab119704d4797bc283257cd3002ac5e0/Applying%20IGBTs\\_5SYA%202053-04.pdf](https://library.e.abb.com/public/ab119704d4797bc283257cd3002ac5e0/Applying%20IGBTs_5SYA%202053-04.pdf)
- [20] Graovac, D. and Pürschel, M. (2009) IGBT Power Losses Calculation Using the Data Sheet Parameters.
- [21] Graovac, D., Pürschel, M. and Andreas, K. (2006) MOSFET Power Losses Calculation Using the Data Sheet Parameters.  
<https://www.element14.com/community/servlet/JiveServlet/download/20553-1-3493/IGBT%20Power%20Losses%20Calculation%20using%20the%20Data%20Sheet%20Parameters.pdf>
- [22] Hermwille, M. (2007) IGBT Driver Calculation.  
<https://www.semikron.com/dl/service-support/downloads/download/semikron-application-note-igbt-driver-calculation-en-2007-10-31-rev-00>



Scientific Research Publishing

**Submit or recommend next manuscript to SCIRP and we will provide best service for you:**

Accepting pre-submission inquiries through Email, Facebook, LinkedIn, Twitter, etc.

A wide selection of journals (inclusive of 9 subjects, more than 200 journals)

Providing 24-hour high-quality service

User-friendly online submission system

Fair and swift peer-review system

Efficient typesetting and proofreading procedure

Display of the result of downloads and visits, as well as the number of cited articles

Maximum dissemination of your research work

Submit your manuscript at: <http://papersubmission.scirp.org/>

Or contact [epe@scirp.org](mailto:epe@scirp.org)